Journal of Maps

ISSN: (Print) (Online) Journal homepage: https://www.tandfonline.com/loi/tjom20

Geology of the Northern Apennines nappe stack on eastern Elba (Italy): new insights on the Neogene orogenic evolution of the Northern Tyrrhenian Sea

Samuele Papeschi, Eric Ryan, Giovanni Musumeci, Francesco Mazzarini, Paolo Stefano Garofalo & Giulio Viola

To cite this article: Samuele Papeschi, Eric Ryan, Giovanni Musumeci, Francesco Mazzarini, Paolo Stefano Garofalo & Giulio Viola (2021) Geology of the Northern Apennines nappe stack on eastern Elba (Italy): new insights on the Neogene orogenic evolution of the Northern Tyrrhenian Sea, Journal of Maps, 17:2, 533-546, DOI: 10.1080/17445647.2021.1972854

To link to this article: https://doi.org/10.1080/17445647.2021.1972854

JOURNAL OF MAPS
2021, VOL. 17, NO. 2, 533–546
https://doi.org/10.1080/17445647.2021.1972854

Geology of the Northern Apennines nappe stack on eastern Elba (Italy): new insights on the Neogene orogenic evolution of the Northern Tyrrhenian Sea

Samuele Papeschi [a], Eric Ryan [b], Giovanni Musumeci [c,d], Francesco Mazzarini [d], Paolo Stefano Garofalo [e] and Giulio Viola [e]

[a]Kochi Institute for Core Sample Research, Institute for Extra-cutting-edge Science and Technology Avant-garde Research (X-star), JAMSTEC, Japan; [b]Department of Geoscience and Petroleum, Norwegian University of Science and Technology, Trondheim, Norway; [c]Dipartimento di Scienze della Terra, Università di Pisa, Pisa, Italy; [d]Istituto Nazionale di Geofisica e Vulcanologia, Pisa, Italy; [e]Department of Biological, Geological and Environmental Sciences, Università degli Studi di Bologna, Bologna, Italy

ABSTRACT

We document the tectonic and metamorphic evolution of thrust nappes of the eastern island of Elba. The area exposes a natural cross section of the Northern Apennines hinterland, from the metamorphic basement units to the overlying continent- and ocean-derived nappes. We integrated mapping, analysis of structures and microstructures, and the interpretation of drill core logs with lithostratigraphic, metamorphic, and geochronological constraints, producing a novel geological map of eastern Elba (1:5'000 scale). We show that the area experienced polyphase Oligocene – Pliocene contractional tectonics marked by in-sequence and out-of-sequence thrusting accompanied by folding and overprinted by faulting in the Pliocene. Magmatism occurred during contraction with post-magmatic thrusting ultimately coupling HP-LT and LP-HT units. Drill core logs allow for the first time the reconstruction of the N-dipping character of the Zuccale Fault, which represents the youngest (late Miocene – early Pliocene) large-scale structure in the area.

ARTICLE HISTORY
Received 17 May 2021
Revised 10 August 2021
Accepted 18 August 2021

KEYWORDS
Geological mapping; structural geology; thrust nappes; drill core interpretation; island of Elba; Northern Apennines

1. Introduction

Thrust wedges are complex systems that originate from the interplay between tectonics, surface processes, and gravitational instabilities (Davis et al., 1983; Dominguez et al., 2000; Ellis et al., 2004; Platt, 1986; Wallis et al., 1993). Integrating geological mapping with metamorphic and geochronological constraints is key to unravel the complex evolution of thrust wedges (e.g. Caso et al., 2021; Di Rosa et al., 2017; Frassi et al., 2016). The Northern Apennines are a classic case study for investigating wedge tectonics (e.g. Clemenzi et al., 2014; Massa et al., 2017; Papeschi et al., 2020a). This E-vergent belt originated after the Neogene collision between Europe and the Adria microplate (Carmignani et al., 1994; Conti et al., 2020). The orogen experienced phases of upper crustal extension and out-of-sequence thrusting, whose contribution to the overall orogenic architecture is debated (Bonini et al., 2014 and references therein).

We present a detailed geological map (Figure 1; Main Map) of the hinterland sector of the belt (eastern Elba) based on an integrated approach combining field mapping with the analysis of drill core logs. We document three different deformation phases (D_1 – D_3) related to in-sequence and out-of-sequence thrusting that led to the coupling between HP-LT and HT-LP metamorphic rocks. The geological data synthetized here contributes to a redefinition of the Oligocene to Pliocene tectono-metamorphic evolution of the Northern Apennines hinterland.

2. Methods

The study area, located between Rio Marina and Porto Azzurro on eastern Elba, covers ~9 km^2. The topographic base is the *Carta Tecnica Regionale – Regione Toscana* (year 1987; raster), which we line-drew to vector format. We conducted a detailed structural-geological survey of the outcropping thrust nappes at the 1:5,000 scale. In order to better document the surface distribution of basement rocks, we do not report thin slope deposits in the resulting map. The mapping workflow included (1) field recognition of lithotypes, formations, and structures, (2) measurement of structural elements (foliations: S; lineations: L; folds: F; fold axes: A), and (3) sample collection and microstructural observations on standard, oriented thin sections, cut parallel to the lineation and perpendicular to the

CONTACT Samuele Papeschi s.papeschi@jamstec.go.jp Kochi Institute for Core Sample Research, Institute for Extra-cutting-edge Science and Technology Avant-garde Research (X-star), JAMSTEC, Japan
Supplemental data for this article can be accessed https://doi.org/10.1080/17445647.2021.1972854.

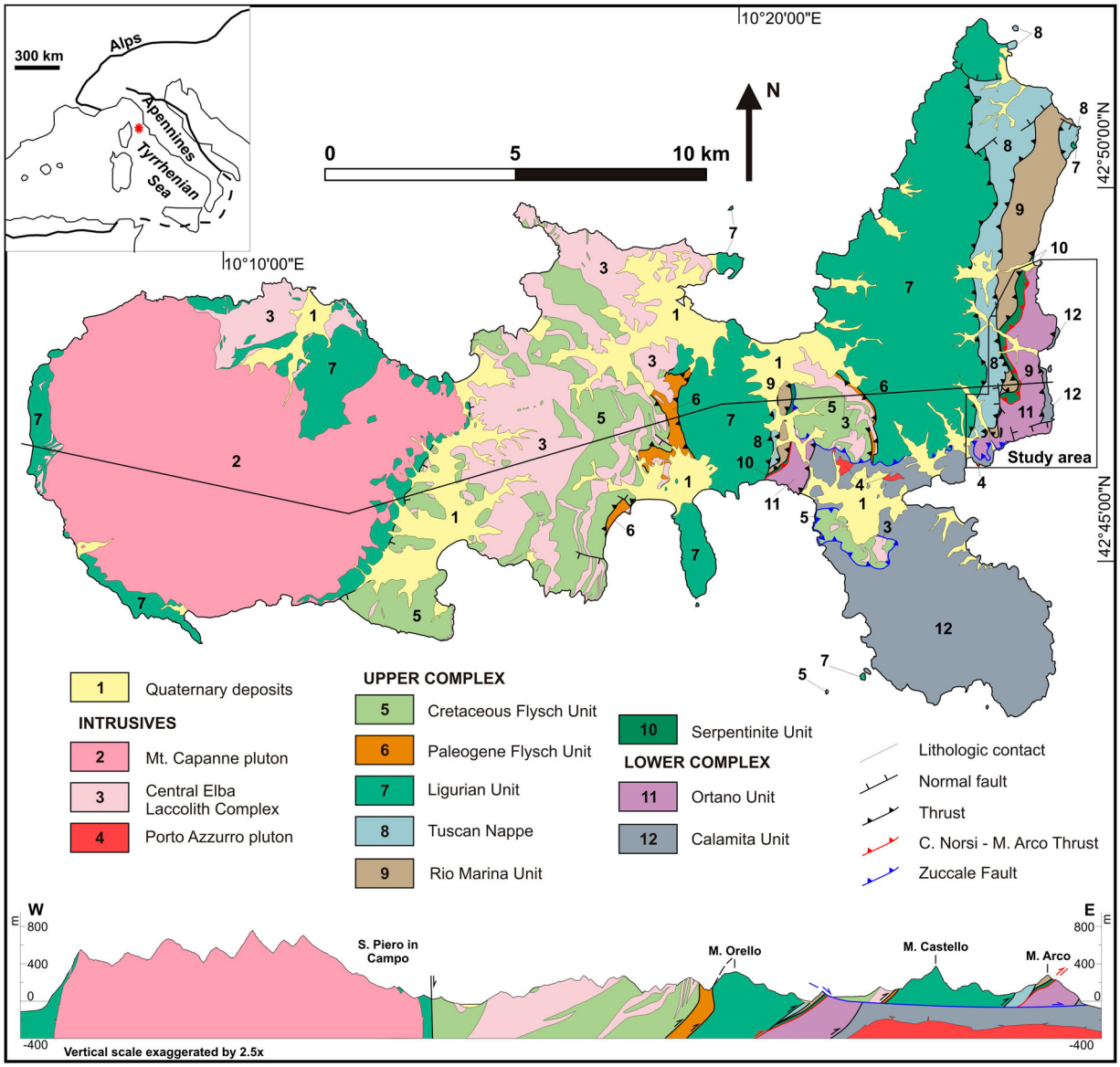

Figure 1. Tectonic sketch map of Elba, including a geological cross section through the nappe stack. Modified after Ryan et al., 2021. Geologic sketch map of the Isle of Elba in the Northern Tyrrhenian Sea.

foliation. We studied over 50 thin sections that allowed us to constrain microstructures and diagnostic metamorphic parageneses. Based on overprinting criteria, metamorphic parageneses, geochronological constraints and structures observed at the meso- to microscale, we defined three deformation phases, referred to as D_1, D_2, and D_3. We refer to the structural elements related to these deformation phases by using a progressive numbering label placed next to the abbreviation of the structural element (e.g. S_1), as it is standard in structural geology (e.g. Ramsay & Huber, 1987). The analysis of 21 commercial drill core logs (location shown on the Main Map) acquired from the Montecatini mining company and locally reaching depths of several hundred meters allowed for a full comparison of the exposed structures (Figure 2) with the subsurface geology (Figure 3). This allowed us to draw several incredibly well constrained cross sections through eastern Elba, where formations have been locally projected down to 500 m below the sea level (Main Map).

3. Geology of eastern elba

The island of Elba (Figure 1) exposes a complete section through the innermost part of the Northern Apennines. Its structure is characterized by WSW-dipping, and ENE-verging tectonic units, accreted during the Oligocene – early Miocene and reworked during the middle-late Miocene (Barberi et al., 1969; Keller & Coward, 1996; Massa et al., 2017; Perrin, 1975; Pertusati et al., 1993; Principi et al., 2015). The units are organized into an Upper Complex, with low- to very-low-grade metamorphism, and a Lower Complex, characterized by two high-grade metamorphic units, preserving relic blueschist-facies parageneses (Bianco et al., 2015, 2019; Papeschi et al., 2020b; Ryan et al., 2021). The two complexes are

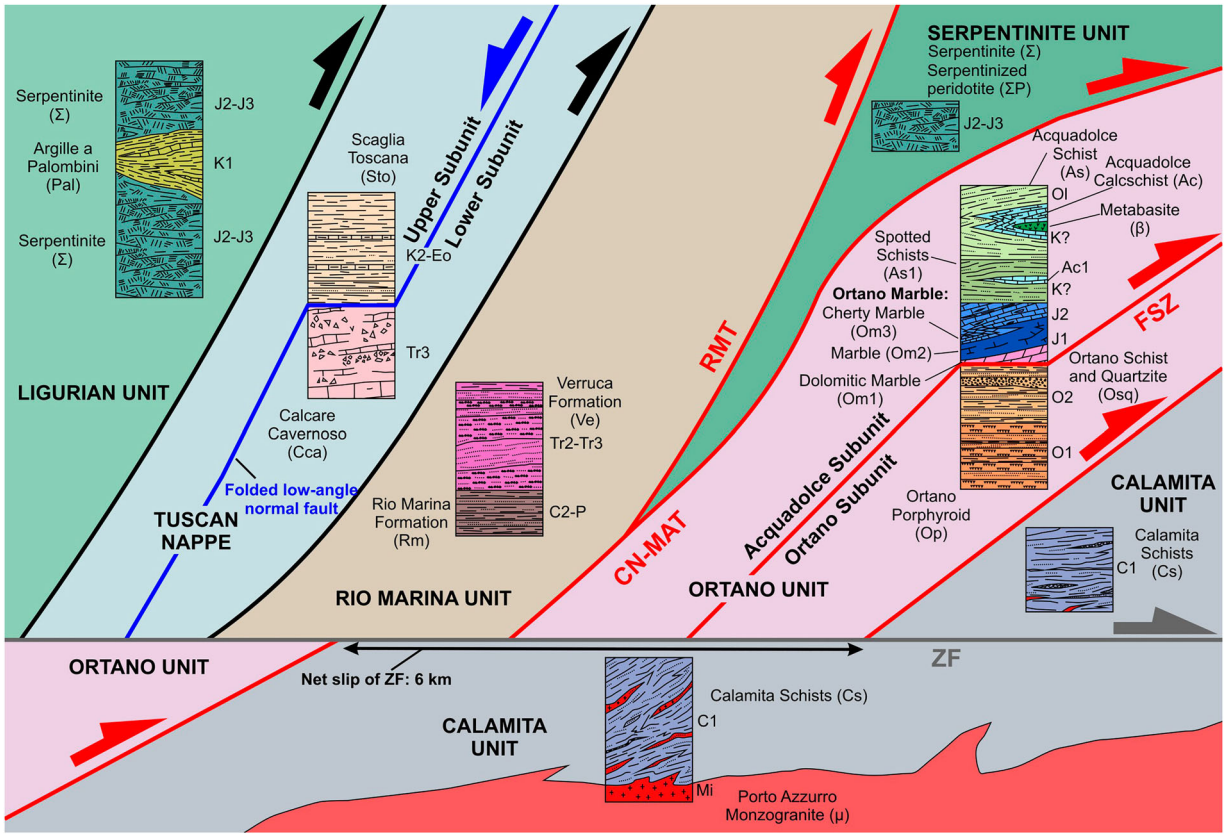

Figure 2. Lithostratigraphy of the eastern Elba nappe stack. Stratigraphic columns are not to scale. D_1 thrusts are shown in black, D_2 low-angle normal faults (refolded) in blue, D_2-D_3 thrusts in red. The Zuccale Fault (post-D_3) is shown in dark grey. Abbreviations of geological time follow Orndorff et al. (2007). Abbreviations of formations are indicated in brackets. Sketch showing the relationships between different rock units in eastern Elba.

separated by the late Miocene Capo Norsi – Monte Arco Thrust (CN-MAT; Viola et al., 2018), marked by a slice of tectonized serpentinites (Figure 1).

Classic models frame the evolution of Elba and the Northern Tyrrhenian Sea in a back-arc geodynamic setting starting in the middle Miocene after early Miocene contraction (Bartole, 1995; Keller & Coward, 1996; Mauffret et al., 1999). However, recent studies show that the nappes recorded thrusting during the late Miocene, after middle Miocene extension at shallow structural levels (Massa et al., 2017). A comprehensive discussion of the two models is beyond the aim of the present study and the reader is referred to Viola et al. (2018) and Ryan et al. (2021) for a more detailed overview of the existing schools of thought. During the late Miocene, plutonic bodies intruded the nappe stack (Dini et al., 2002; Marinelli, 1959). The Porto Azzurro Pluton, emplaced underneath eastern Elba, caused LP-HT metamorphism at $P < 0.2$ GPa on the Lower Complex (Duranti et al., 1992; Musumeci & Vaselli, 2012). E-verging thrusts and coeval late Miocene LP-HT metamorphism reworked the nappe stack, leading to the coupling between the Upper Complex, largely unaffected by contact metamorphism, with the Lower Complex (Figure 1; Massa et al., 2017). The late Miocene – early Pliocene Zuccale Fault (ZF) crosscuts this nappe stack, displacing it by 6 km to the east (Figure 2). Early authors classically interpreted the ZF as a low-angle normal fault (Collettini & Holdsworth, 2004; Keller & Pialli, 1990) but, more recently, Musumeci et al. (2015) and Viola et al. (2018) proposed an alternative view of it as an out-of-sequence thrust. High-angle normal faults and strike-slip faults have formed since the Pliocene (Figure 1; Main Map; e.g. Mazzarini et al., 2019).

4. Lithostratigraphy, metamorphism, and magmatism

4.1. Upper Complex

4.1.1. Ligurian Unit and Serpentinite Unit

The Ligurian Unit comprises several oceanic anchizone-facies nappes (Barberi et al., 1967a, 1969; Conti et al., 2020; Perrin, 1975; Reutter & Spohn, 1982). The unit preserves a Middle-Upper Jurassic ophiolite complex overlain by Upper Jurassic – Lower Cretaceous pelagic sequences. In the study area, serpentinized peridotite (*Serpentinite*; Figure 2) with lherzolite to harzburgite composition (Viti & Mellini, 1998) occur at the base of the Ligurian Unit and as a slice sandwiched between continental units (Serpentinite Unit; Figure 2). Hauterivian – Albian shales with limestone

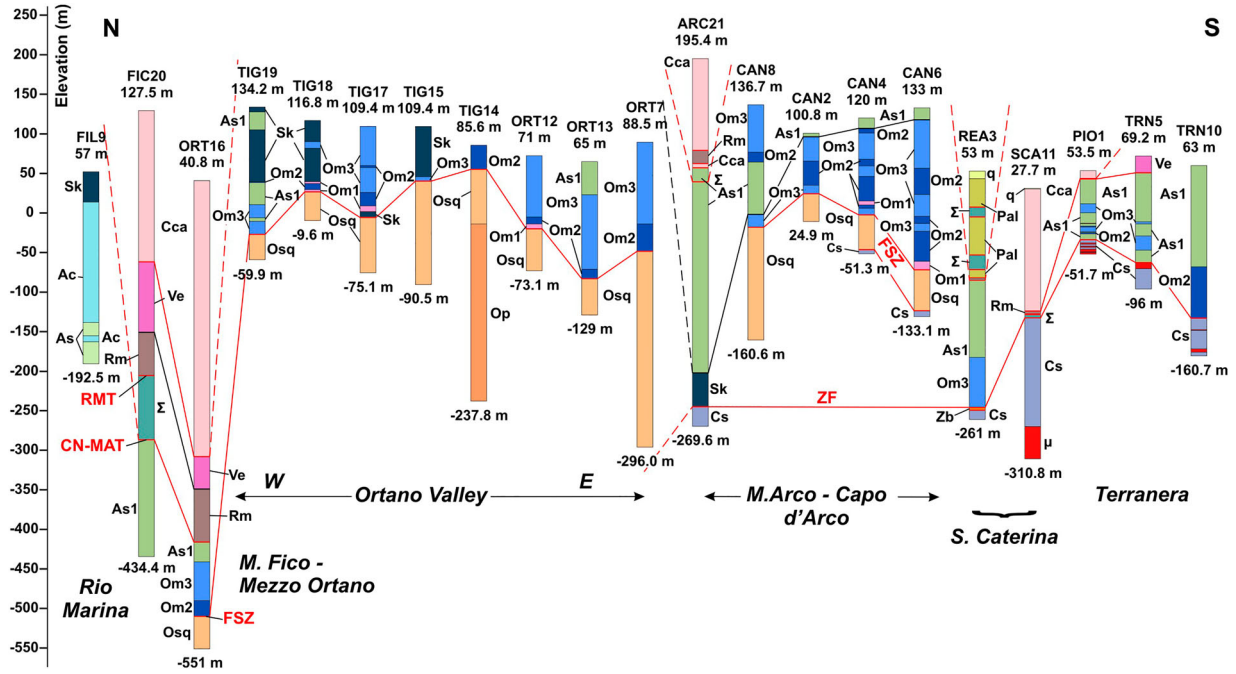

Figure 3. Interpretation of the subsurface geology based on drill core logs. Abbreviations of formation are shown in Fig. 2. Correlation and sketch the drill core logs from the study area.

layers (*Argille a Palombini* Fm.), originated from the oceanic sequences, occur as slices within the serpentinites to the south-west of the study area (Main Map).

4.1.2. Tuscan Nappe

The anchizone-facies Tuscan Nappe (Figure 2) consists of Mesozoic-Cenozoic passive margin sequences (e.g. Conti et al., 2020). In the study area, the Tuscan Nappe is tectonically reduced (Serie Ridotta; Decandia et al., 1993; Perrin, 1975; Trevisan, 1950). Massa et al. (2017) recognized a Lower and an Upper Subunit, separated by a synorogenic low-angle normal fault (Figure 2). The Lower Subunit consists of the *Calcare Cavernoso* Fm. (Barberi et al., 1969), a limestone tectonic breccia derived from original Norian evaporite (e.g. Burckhardt, 1946). The Upper Subunit contains the *Scaglia Toscana* Fm., a sequence of varicolored slate, siltstone, and marl of hemipelagic environment with Maastrichtian – Eocene microfauna (Keller & Pialli, 1990; Perrin & Neumann, 1970).

4.1.3. Rio Marina Unit

The Rio Marina Unit (Figure 2) is a lower greenschist-facies (Franceschelli et al., 1986) continental unit comprising (1) the Upper Carboniferous – Permian Rio Marina Fm. and the (2) Middle-Upper Triassic Verruca Fm. (Figure 2; Barberi et al., 1967a; Perrin, 1975). The Rio Marina Fm. consists of interlayered graphitic phyllite, metasiltstone, and metasandstone, with lenses of metaconglomerate, referred to a coastal – deltaic environment of Westphalian – Stephanian/Autunian age (Bodechtel, 1964; De Stefani, 1914; Deschamps et al., 1983; Perrin, 1975). The Verruca Fm. consists of violet phyllite, quartzite and quartz-rich conglomerate (*Anageniti Auctt.*) of alluvial plain environment, belonging at regional scale to the Verrucano Group (Cassinis et al., 2018).

4.2. Lower Complex

4.2.1. Ortano Unit

The Ortano Unit (Figure 2) is a complex of tectonic slices derived from a Paleozoic basement (Ortano Subunit) and a Mesozoic – Cenozoic sequence (Acquadolce Subunit), separated by the late Miocene Felciaio Shear Zone (FSZ; Duranti et al., 1992; Musumeci & Vaselli, 2012). The Ortano Unit experienced early Miocene blueschist-greenschist-facies metamorphism, preserved to the north (HP-LT Complex in Main Map; Papeschi et al., 2020b; Ryan et al., 2021) and late Miocene amphibolite-facies metamorphism, pervasive over the rest of the Ortano Unit (LP-HT Complex in Main Map).

The Ortano Subunit (Figure 2) comprises the Ortano Porphyroid, a sequence of quartz-feldspar-biotite-bearing metavolcanite and metasandstone, and the Ortano Schist and Quartzite, cordierite-andalusite-biotite-bearing schist, metasandstone, and metaconglomerate. Lithostratigraphic features and U-Pb zircon ages support the correlation of the Ortano Porphyroid with Variscan Middle Ordovician volcano-sedimentary sequences. The Ortano Schist and Quartzite is correlated with Upper Ordovician trangressive deposits, also based on Ordovician –

early Silurian detrital zircon ages (Bortolotti et al., 2001; Duranti et al., 1992; Musumeci et al., 2011; Sirevaag et al., 2016).

The Acquadolce Subunit (Figure 2) comprises the Ortano Marble and the Acquadolce Schist (Duranti et al., 1992; Massa et al., 2017). The Ortano Marble is a mylonitized sequence with cataclasite at the base, marking the FSZ and comprising: (1) lenses of dolomite marble (Dolomitic Marble), (2) diopside-tremolite-talc-bearing massive marble (Marble), and (3) calcschist and cherty marble (Cherty Marble). The Ortano Marble correlates with the Hettangian – Bathonian carbonate sequences of the Tuscan Domain (Barberi et al., 1969; Duranti et al., 1992; Massa et al., 2017). The Acquadolce Schist is a metapelitic-metapsammitic sequence with bodies of metacarbonates (Acquadolce Calcschist) and lenses of metabasites (Metabasite) of unknown age (tentatively attributed to the Cretaceous by Massa et al., 2017). The metabasic bodies preserve relic lawsonite pseudomorphs, glaucophane, and omphacite, indicating peak $P > 1.5$ GPa (Papeschi et al., 2020b). White mica from the associated calcschists yielded early Miocene ages (Ryan et al., 2021 and references therein). South of Monte Fico – Il Porticciolo (Main Map), LP-HT biotite-cordierite-andalusite parageneses in metapelites (Spotted Schists) and tremolite-diopside-talc in metacarbonates (Contact-metamorphosed Calcschist) replace the regional metamorphic assemblages (Duranti et al., 1992; Musumeci & Vaselli, 2012; Papeschi et al., 2020b). The Spotted Schists correlate with Oligocene foredeep deposits of the Northern Apennines, based on U-Pb detrital zircon ages (Jacobs et al., 2018; Massa et al., 2017).

4.2.2. Calamita Unit

The Calamita Unit (Figure 2), in the study area, consists only of the Calamita Schists, a high-grade schistose complex derived from Lower Carboniferous (Visean) Flysch (Barberi et al., 1967b; Musumeci et al., 2011; Papeschi et al., 2017, 2018). The Calamita Schists are biotite + cordierite + andalusite + K-feldspar ± plagioclase ± white mica paragneiss, schist, and quartzite that experienced peak T > 650–700 °C at $P < 0.2$ GPa in the late Miocene (Duranti et al., 1992; Musumeci et al., 2015; Musumeci & Vaselli, 2012; Papeschi et al., 2019). The outcrops on the eastern coast of the study area, formerly known as the Capo d'Arco Schists, were recently correlated with the Calamita Schists (Massa et al., 2017; Mazzarini et al., 2011).

4.2.3. Porto Azzurro pluton

The Calamita Unit hosts the Upper Miocene Porto Azzurro pluton (Figure 2). The main intrusive body is buried at 100-200 m depth and crops out only as scattered biotite-tourmaline monzogranite apophyses and as a swarm of coeval leucogranite and pegmatite dykes and sills (Marinelli, 1959; Mazzarini et al., 2011; Mazzarini & Musumeci, 2008). The distribution of LP-HT metamorphism indicates a ~60 km^2 areal extent of the pluton, supported by gravimetric profiles (Musumeci & Vaselli, 2012; Siniscalchi et al., 2008).

4.3. Metasomatic rocks

Elba hosts several Fe-oxide deposits that have constituted an important mining district since ancient times (Tanelli et al., 2001). The Fe production of the entire district is estimated to be between 83 and 88 Mt of ore (Zitzmann, 1977). These deposits, dated to ~ 5–6 Ma, are roughly coeval with magmatism (Lippolt et al., 1995; Maineri et al., 2003). The Rio Marina mine (immediately to the north of our study area) is the largest of the district and contains massive hematite-pyrite ore bodies hosted by the Rio Marina Unit (Deschamps et al., 1983; Tanelli et al., 2001). The mineral association comprises minor magnetite, chalcopyrite, sphalerite, adularia, quartz, and rare fluorite. The deposits of the Ortano Valley (Main Map) show a peculiar pyrite + pyrrhotite ± hematite ± magnetite association (Tanelli et al., 2001). The mineralizations of Rio Marina and Ortano occur together with skarns (Main Map), developed primarily in carbonatic lithologies and showing the distinctive hedenbergite + ilvaite + epidote ± quartz ± chlorite assemblage. The Terranera deposit (Main Map) consists of metric to decametric lenses of hematite-goethite hosted within the Zuccale Fault (Dünkel, 2002). Ore minerals and secondary relict magnetite and pyrite occur within a chlorite- and clay minerals-rich matrix. Between Terranera and Punta delle Cannelle, mineralizations are associated with skarns in schistose lithologies.

5. Tectono-metamorphic evolution of eastern elba

The tectonic lineaments (thrusts, shear zones, and faults) and main foliation in eastern Elba strike dominantly N–S to NNW–SSE and dip to the WSW, with a local NNE–SSW strike in the study area (stereonets on the Main Map). Fold axes show a dominant NW–SE Apenninic orientation with only local variations (Keller & Coward, 1996; Massa et al., 2017). Stretching lineations trend E–W to NE–SW (Main Map: stereonet f). We reconstruct a tectonic evolution marked by three deformation phases, labeled D_1 to D_3.

5.1. Deformation phases

5.1.1. D_1 phase: early Miocene nappe stacking and exhumation

Structures associated with the D_1 phase (Figure 4) occur in the Upper Complex and in the HP-LT portion of the Acquadolce Subunit. D_1 structures, related to early Miocene nappe stacking (Massa et al., 2017),

show a N–S striking and WNW-WSW-dipping penetrative S_1 foliation (Main Map: stereonet a) associated with anchizone to lower greenschist-facies metamorphism in the Upper Complex (Figure 4(a, b) and greenschist-blueschist-facies metamorphism in the Acquadolce Subunit (Lower Complex; Figure 4(c, d)). A_1 axes, striking NNW-SSE and plunging gently to the NW and SE, are associated with tight to isoclinal non-cylindrical intrafolial F_1 folds (Main Map: stereonet b). Calcite and quartz fibers and rods, and trails of phyllosilicates mark the L_1 stretching lineations, which dominantly trend ENE-WSW. In the Upper Complex, oriented white mica + chlorite ± graphite and quartz-/carbonate-layers in metapelites define the S_1 slaty cleavage (Figure 4(a)). In serpentinites, oriented serpentine and elongated relics of olivine, clinopyroxene, and orthopyroxene define the S_1 foliation (Figure 4 (b)), whereas the stretching lineation is marked by serpentine fibers. Predominantly in the area of Monte Arco (Main Map), serpentinites contain large bodies of peridotite that preserve pre-orogenic HT fabrics and mylonitic structures that we relate to the Jurassic

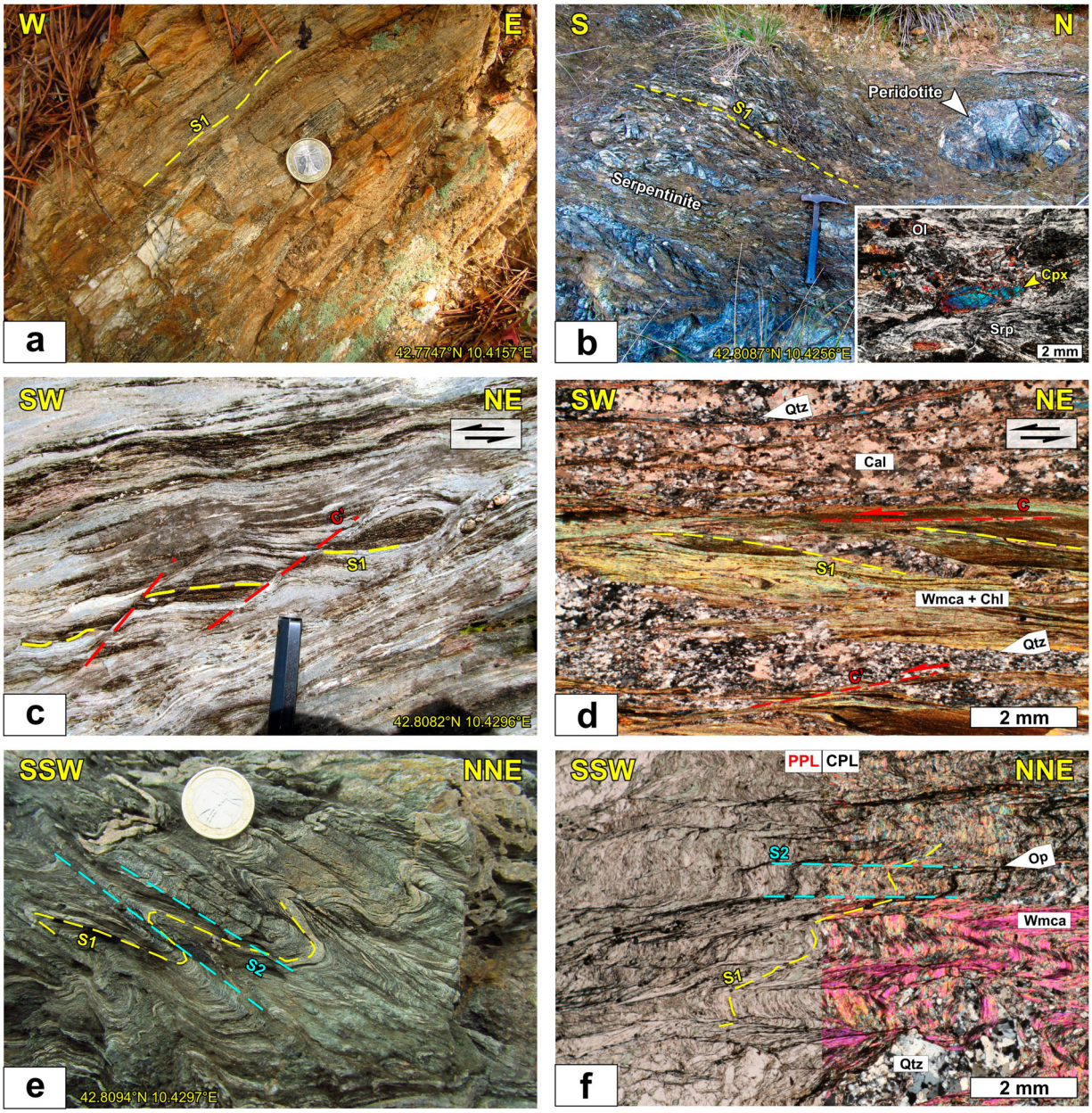

Figure 4. Deformation structures produced by D_1 and D_2 phases. **(a)** W-dipping S_1 foliation in quartzite and phyllite of the Verrucano Fm. **(b)** Serpentinite showing a foliated fabric with lenses of less-foliated peridotite. The insert shows olivine and pyroxene relics surrounded by foliated serpentine (CPL: crossed polarized light). **(c)** Foliated marble with chert nodules and top-to-the-W S-C′ structures (Acquadolce Calcschist). **(d)** Microphotograph of the Acquadolce Schist showing the S_1 foliation, defined by white mica and chlorite, reworked by top-to-the-W S-C′ structures. **(e)** Mesoscale and **(f)** microscale image of crenulated fabric (S_1-S_2) showing local SSW vergence in the Acquadolce Calcschist (CPL and PPL: Plane Polarized Light). Mineral abbreviations after Siivola and Schmid (2007). Images of rock structures produced by the first and second deformation phases in the eastern Elba nappe stack.

oceanic spreading stage, recently documented in the ophiolites of western Elba (Frassi et al., 2017).

In the Acquadolce Subunit, a continuous schistosity defines the S_1, marked by the metamorphic layering (Figure 4(c)) and the preferred orientation of white mica, calcite, glaucophane, actinolite, albite, and epidote (Figure 4(d); Papeschi et al., 2020b and Ryan et al., 2021). The Acquadolce Subunit recorded blueschist- to greenschist-facies W-directed shearing with the development of mylonitic shear zones, containing several kinematic indicators consistent with top-to-the-W kinematics (Figure 4(d)), related to syn-orogenic exhumation that likely transposed pre-existing underplating-related structures (Ryan et al., 2021). F_1 folds in the Acquadolce Subunit are small intrafoliar to decimeter-scale structures with non-cylindrical to sheath-like geometry, showing A_1 axes completely scattered on foliation planes (Main Map: stereonet d).

5.1.2. D_2 phase: middle-late Miocene folding

The development of the Rio Marina Antiform, a km-scale east-facing overturned nappe antiform (F_2) whose hinge zone is exposed further north, outside of the study area, marks the D_2 deformation phase (Massa et al., 2017). The study area exposes the reverse limb of this structure, marked by a sheared tectonic slice of serpentinite and peridotite (Serpentinite Unit) derived from the overlying Ligurian Unit and sandwiched between two middle-late Miocene thrusts (RMT and CN-MAT; see below). S_2 foliation is an axial plane crenulation cleavage with millimetric to centimetric spacing that affects the less competent lithologies of the Upper Complex and the Acquadolce Subunit (Figure 4(e, f)). The S_2 generally strikes NW-SE and dips gently to the W, with local northward, eastward, and southward dips (Main Map: stereonet e). It is associated with open to tight non-cylindrical recumbent to inclined F_2 folds, developed in the more competent layers (Figure 4(e)).

At the microscale, the S_2 foliation is a gradational to discrete crenulation cleavage defined by opaque-rich (pyrite, graphite) pressure solution surfaces and re-oriented white mica and chlorite grains (Figure 4). Local contact metamorphic parageneses, represented by biotite, chlorite, and rare oligoclase are present in dissolution seams and fractures that crosscut the S_2 foliation or as static flakes overgrowing it, indicating that D_2 folding and crenulation predates the LP-HT event, in agreement with Massa et al., 2017.

5.1.3. D_3 phase: late Miocene syn-magmatic thrusting

D_3 structures (Figure 5) are linked to late Miocene LP-HT metamorphism, pluton emplacement, and coeval regional deformation in the Lower Complex (LP-HT Complex), where they constitute its dominant mesoscale fabric. The S_3 foliation strikes dominantly N-S and dips to the W (Figure 5(a, b, c); Main Map: stereonet c), being parallel to the S_1 in the Upper Complex and the HP-LT part of the Acquadolce Subunit (Figure 5). At map scale, the coupling between the D_1-D_2 structures in the Upper Complex and the D_3 structures in the Lower Complex is through tectonic contacts (i.e. CN-MAT; Main Map). Within the Acquadolce Subunit, extremely condensed metamorphic isograds related to ductile shearing, mark the transition between the northernmost glaucophane-bearing and the southern andalusite-bearing metamorphic rocks (e.g. Figure 5(a); Papeschi et al., 2020b). The S_3 foliation is a continuous schistosity defined by the preferred orientation of medium- to high-grade metamorphic assemblages (white mica, biotite, cordierite, andalusite in metapelite: Figure 5 (d, e); diopside, tremolite, talc in marble and dolomitic marble), the metamorphic layering (Figure 5(b)), and deformed objects, such as clasts in metaconglomerate (Figure 5(c)). Schistose lithologies commonly show late NS-striking and W-dipping crenulations of the S_3 foliation, formed during retrograde conditions and marked at the microscale by opaque-rich surfaces. These crenulations are associated, at map scale, with large antiforms and synforms of foliation occurring in the Monte Arco area (Main Map). Oriented mineral grains and aggregates (biotite, white mica, andalusite, cordierite, tremolite, and calcite), and stretched objects (clasts in metaconglomerate: Figure 5(c); feldspar grains in the Ortano Porphyroid) outline NE–SW trending L_3 stretching lineations (Main Map: stereonet f). F_3 folds are non-cylindrical tight to isoclinal intrafolial to decimeter-scale structures with dispersed A_3 axes (Main Map: stereonet d) outlined by deformed quartz-rich layers in metapelites and refolded carbonate-rich layers in marbles. At map scale, the Ortano marble defines large F_3 structures, isoclinally folded within the Spotted Schists (Main Map). These structures likely represent earlier F_1 folds reworked during the D_3 phase. L_3 lineations show constant trends on the surface of the folds, indicating sheath-like geometry. The competent Ortano Porphyroid preserves coarse-grained K-feldspar, plagioclase, and quartz-clast and layers associated with a very fine-grained white mica + biotite foliation. We interpret this fabric as a S_1 foliation only slightly overprinted by LP-HT metamorphism, lacking evidence of significant late Miocene deformation.

D_3 ductile shearing localized in the meter-thick marble at the base of the Ortano Marble and in anastomosing cm- to dm-thick shear zones in the Spotted Schists and the Calamita Schists andalusite-cordierite-bearing metapelites (e.g. Figure 5(d)). Shear zones anastomose through low-strain lenses that show poorly foliated to hornfels-like fabric with relic folds (e.g. Figure 5(e)). Kinematic indicators (i.e. S–C structures, oblique foliations,

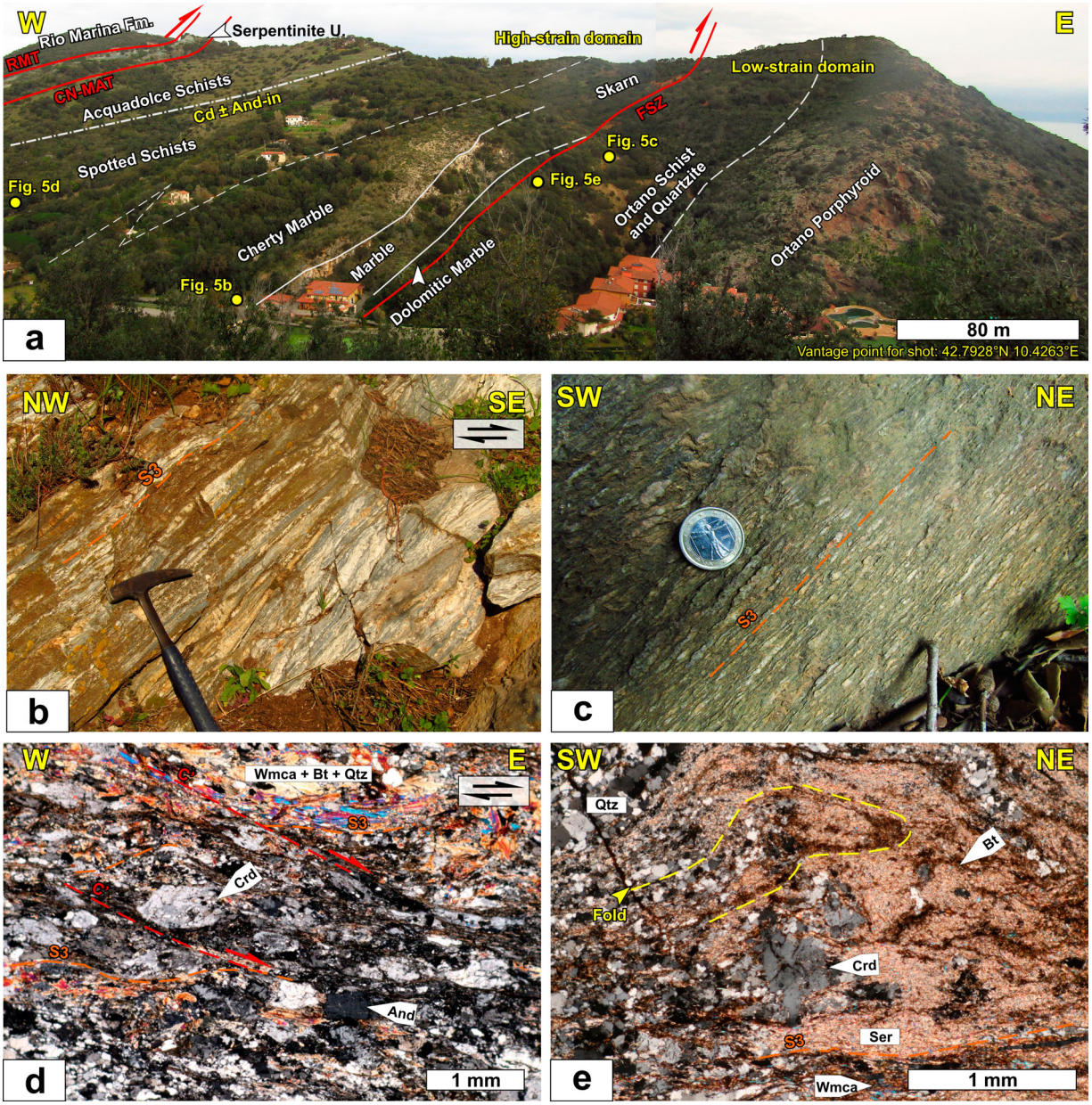

Figure 5. D_3 structures. **(a)** Section through the Ortano Valley revealing major tectonic structures and the relationships between the Upper and Lower Complexes. **(b)** Foliated Ortano Marble (Cherty Marble) with boudinaged metachert, truncated by synthetic and antithetic top-to-the-E structures. **(c)** Metaconglomerate (Ortano Schist and Quartzite) displaying a strongly SW-NE-oriented lineated fabric. **(d)** Spotted Schist with coarse-grained white mica, cordierite, and andalusite, crosscut by top-to-the-E mylonitic bands (CPL). **(e)** Schist showing a folded, weakly foliated fabric, defined by quartz and biotite layers, associated with large grains of cordierite and intense sericitization (CPL; Ortano Schist and Quartzite). Mineral abbreviations after Siivola and Schmid (2007) Images of rock structures produced by the third deformation phase within the eastern Elba nappe stack.

asymmetric porphyroblasts, and mica fishes; e.g. Figure 5) are all consistent with top-to-the-E kinematics. Available age constraints indicate 6.1–6.7 Ma ages for the synkinematic minerals on the S_3 foliation (Musumeci et al., 2015; Musumeci & Vaselli, 2012; Viola et al., 2018).

5.2. Thrust faults and shear zones

5.2.1. Rio Marina thrust (RMT) and Capo Norsi-Monte Arco thrust (CN-MAT)

The N-S striking and W-dipping RMT and CN-MAT record a polyphase D_2 – D_3 activity that led to the thrusting of the Upper Complex over the Lower Complex. During the D_2 phase, these thrusts accommodated shearing on the reverse limb of the Rio Marina Antiform (Massa et al., 2017). They slipped again in the late stages of the D_3, superimposing non-contact metamorphic rocks over the Lower Complex (Musumeci & Vaselli, 2012; Viola et al., 2018). North of Monte Arco, the two faults localize at the top and the bottom of the Serpentinite Unit respectively (Main Map). South of Monte Arco, the Serpentinite Unit progressively tapers and the RMT and CN-MAT splay into a series of minor thrusts affecting the Serpentinite, the Spotted Schists, the Rio Marina

Unit and the *Calcare Cavernoso* Fm. (Figure 6(a)). In this area, a slice of medium grade Spotted Schists are tectonically sandwiched between the Serpentinite Unit and the Rio Marina unit (Figure 6(a)). Further west, in the Fosso Reale creek (Main Map), the non-metamorphic *Calcare Cavernoso* overlies and occurs as slices within the metamorphic Spotted Schists (Figure 6(b,c)). Serpentinites occur as tectonized lenses within the Spotted Schists in Terranera, where cataclasite (Figure 6(d)) and intense carbonate veining (Figure 6(e)) overprint D_1 structures. Field relationships are consistent with the latest brittle movements of the CN-MAT, dated to 4.9 ± 0.27 Ma by Viola et al. (2018).

5.2.2. Felciaio shear zone (FSZ)

The FSZ is a NS-trending and W-dipping D_3 ductile shear zone localized in the Ortano Marble (Figure 5 (a, b); Main Map), marking the contact between the Acquadolce Subunit and the underlying Ortano Subunit (Musumeci & Vaselli, 2012). The FSZ consist of diopside-tremolite-bearing mylonitic marble and

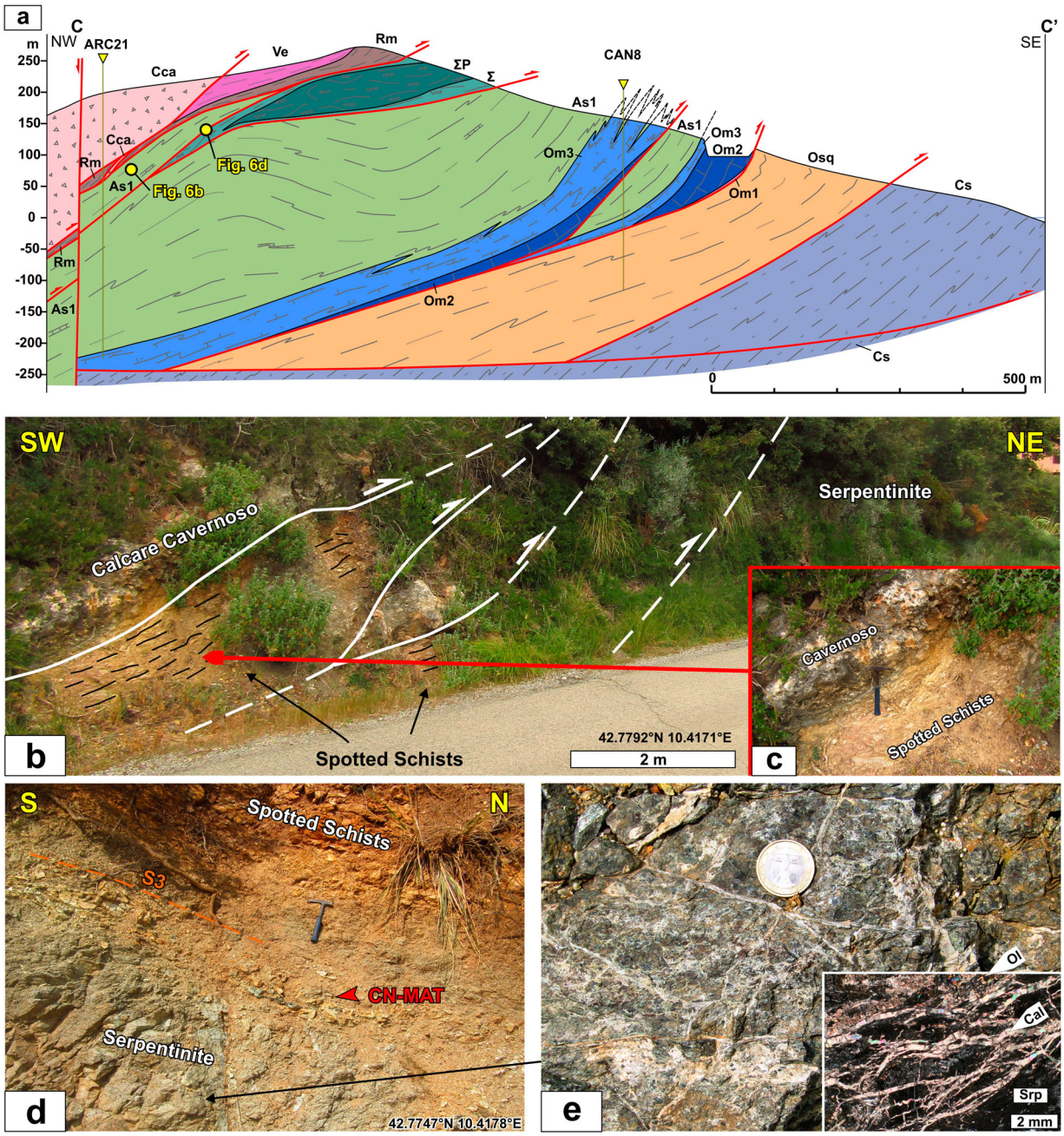

Figure 6. Architecture of out-of-sequence thrust faults in eastern Elba. **(a)** Cross section through Monte Arco (Main Map). **(b)** Road cut view with **(c)** detail of multiple horses of Calcare Cavernoso and Spotted Schists in the splay area of the CN-MAT and RMT. **(d)** Exposure of the CN-MAT thrusting the Spotted Schists onto the serpentinite in Terranera. Note the strong cataclastic overprint of both lithologies. **(e)** Cataclastic overprint of the serpentinite, marked by calcite-filled veins and fractures. The insert shows the same features at the microscale (CPL). Mineral abbreviations after Siivola and Schmid (2007). Abbreviations of formations following Fig. 2. Schematic cross section through Monte Arco and images of rock structures associated with brittle thrust faults.

calcschist with sheared chert and calcsilicate nodules, displaying top-to-the-E kinematics (folds, S–C structures, oblique foliations; Figure 5(b)). This structure brings medium- to high-grade rocks (cordierite/andalusite-schist; diopside/tremolite-marble) over the low-medium grade Ortano Porphyroid (biotite + white mica; Musumeci & Vaselli, 2012). Field relationships and geochronological data (6.7 - 6.2 Ma) constrain the activity of this structures to the late Miocene LP-HT metamorphic event, indicating crustal shortening during the emplacement of Porto Azzurro pluton.

5.3. Zuccale Fault (ZF)

The ZF (Figure 7(a)) is a top-to-the east subhorizontal brittle fault truncating all previous tectonic structures (post-D_3) with a net slip of 6 km (Figure 2), based on the displacement of earlier thrust faults in its footwall and hanging wall (e.g. Keller & Pialli, 1990). We re-interpret the ZF as an out-of-sequence thrust, following Musumeci et al. (2015). The ZF was recently constrained to the early Pliocene by K/Ar dating of authigenic and synkinematic illite separated from a variety of ZF rocks (post 4.9 Ma; Viola et al., 2018). In the study area, the ZF brings the Upper and Lower Complex in the hanging wall over the Calamita Unit (Main Map). The fault zone crops out in Terranera (Figure 7(a)). Here, the ZF is expressed by a 5 m thick fault core and separates the Spotted Schists (hanging wall) from the Calamita Schists (footwall). The fault core contains lenses of footwall and hanging wall-derived lithologies (e.g. leucogranite, schist, basalt), including a large lens of mylonitic marble derived from the Ortano Marble (Figure 7(b)) preserving structures related to the FSZ (dated to 6.7 Ma; Musumeci et al., 2015). Fault rocks consist of poorly lithified to loose fault-breccia, cataclasite and fault gouge with heterometric fragments and slices of footwall and hanging wall lithologies (schist, leucogranite, marble, basalt, serpentinite), surrounded by a clay-rich

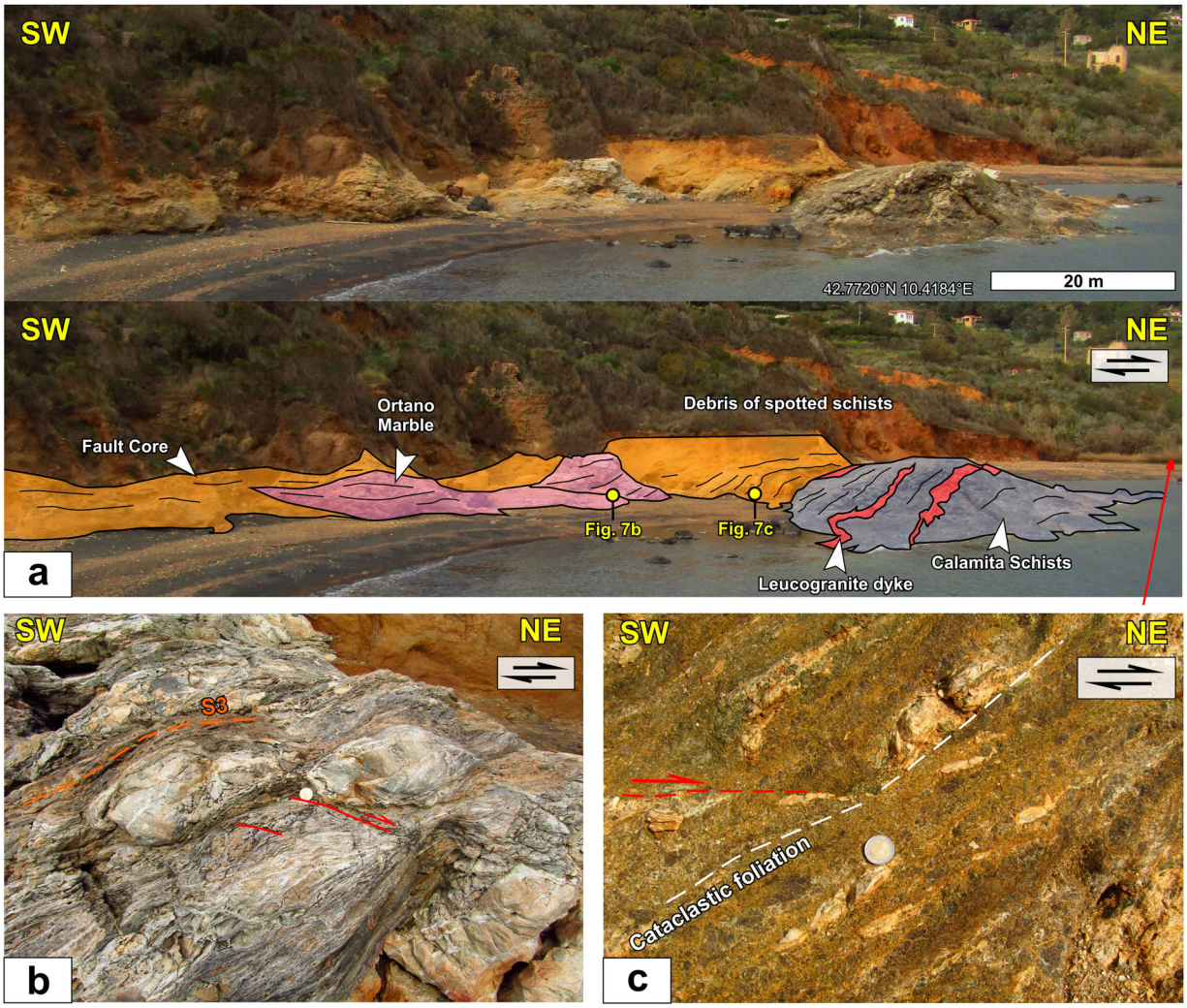

Figure 7. Zuccale Fault. **(a)** Panorama of the fault zone in Terranera. **(b)** Detail of the lens of mylonite marble, originated from the Ortano Marble. Top-to-the-E shear bands are well visible. **(c)** Detail of the fault core, consisting of a heterogeneous foliated cataclasite with fragments of schist, marble, and granite (predominantly). Images of rock structures associated to the Zuccale Fault in Terranera (Elba).

matrix (Figure 7(c)). They show a well-defined cataclastic foliation, outlined by a preferred orientation of trails of fragments and a varicolor, foliated matrix, locally crosscut by top-to-the-E synthetic shears (Figure 7). E-W-trending slickenlines are visible in the fault core as calcite, quartz, and hematite fibers, and trails of phyllosilicates on sheared surfaces. Fe-oxide and sulphide mineralizations permeate the matrix overprinting the cataclastic fabric, indicating that the fault acted as a preferential fluid pathway (Gundlach-Graham et al., 2018).

5.3.1. Pliocene - Quaternary faults

Pliocene – Pleistocene tectonics (post-ZF) consist of a dominant system of N-S striking, subvertical normal faults that overprint earlier W-dipping thrusts with displacements up to ~150 meters (Main Map). Most faults show down-dip slickenlines, marked by calcite and quartz fibers. Hydrothermal alteration often permeates fault cores depositing iron oxides, chlorite, and epidote. Locally, E-W trending, vertical, left-lateral strike-slip shear zones show displacements ranging from a few meters to several hundred meters, as between Terranera and Punta delle Cannelle (Main Map). At the latter locality, the deposition of skarn deposits and mineralizations (Fe-pargasite skarn, chloritite, and epidosite) accompanies strike-slip tectonics and the regional foliation bends in parallelism with transcurrent faults.

6. Drill core interpretation

Drill core logs highlight a W-dipping monoclinal structure encompassing the entire study area down to a depth of 500-600 m (Figure 3). Lateral variations in unit thickness can be ascribed primarily to thrusts, encountered by drillings and visible at outcrop scale. For example, the Serpentinite Unit disappears as a series of tectonic slices to the south, as observed in the field (Figure 6) and in drill core logs (e.g. ARC21, REA3, SCA11; Figure 3). Normal faults have limited control on the large-scale geometry, showing limited displacements (~ 150 m) and mostly reactivating former thrusts (e.g. section B-B' in Main Map).

The drillings to the south (e.g. ARC21, REA3; SCA11; PIO1; Figure 3) document the contact between the hanging wall (mostly Acquadolce Subunit) and footwall (Calamita Schists) of the ZF. The depth of the ZF increases regularly from S to N with a N to NNE average dip of 7–11 °, based on both field relationships and drill core log constraints (Figure 3).

7. Conclusions

Detailed field surveying, coupled with structural analysis, petrographic investigations, and interpretation of drill core logs, allowed the realization of a novel 1:5,000 scale geological map of the eastern Elba nappe stack, providing new insights into its tectono-metamorphic evolution. The geological map offers an updated overview of the lithostratigraphic, tectonic, and metamorphic features of eastern Elba. Consistently with recent studies, we document:

1) early Miocene top-to-the-E nappe stacking and top-to-the-W exhumation related structures, defining the first-order nappe pile;
2) middle-late Miocene out-of-sequence thrusts, coeval with magmatism, that reworked the nappe stack in a key sector of the inner Northern Apennines;
3) the hierarchy and correlation of tectonic structures across different tectonic units, leading to the definition of three deformation phases;
4) the deep architecture of Elba.

Data

The list of the samples used in the present study is provided as supplementary material to the present article. The list includes the sample name (registered as IGSN on SESAR: www.geosamples.org), its assemblage, accessories, and classification. Drill core logs, interpreted as an integral part of this study, are freely available on the repository of the Tuscany Region at http://www502.regione.toscana.it/geoscopio/geologia.html.

Software

The original raster has been geo-referenced on QGIS 3.16.0 and converted to vector format using CorelDraw X4. We used the software Stereonet 11 (https://www.rickallmendinger.net/) and OpenStereo (Grohmann & Campanha, 2010) to plot the measured structural elements in equal area, lower hemisphere stereographic projections, shown on the Main Map.

Geolocation information

The study area is located on eastern Elba, between Rio Marina and Porto Azzurro, in the Tuscan Archipelago (Italy). The area lies within 615093mE – 4735873mN and 617544mE – 4741376mN; coordinate system: WGS84 / UTM Zone 32 T.

Acknowledgements

We thank Espen Torgersen for the many fruitful and stimulating discussions in the field. We also thank Mike Smith and Arthur Merschat for their editorial job, Chris Orton for his cartographic review, and Stefano Vitale and Gianluca Cornamusini for their technical reviews that helped improving the quality of the map and the associated manuscript.

Disclosure statement

No potential conflict of interest was reported by the author(s).

Funding

This work was funded by PRA 2018/2019 of the University of Pisa (PI: G. Musumeci/C. Pagli), FISR2016 INGV Bottom-up (PI: F. Mazzarini), and the Fault Fluid grant issued by Consorzio Nazionale per l'Ingegneria delle Georisorse (PI: P.S. Garofalo).

ORCID

Samuele Papeschi http://orcid.org/0000-0002-5774-7119
Eric Ryan http://orcid.org/0000-0003-3827-4405
Giovanni Musumeci http://orcid.org/0000-0001-5343-4708
Francesco Mazzarini http://orcid.org/0000-0002-3864-6558
Paolo Stefano Garofalo http://orcid.org/0000-0001-5414-0103
Giulio Viola http://orcid.org/0000-0002-8383-3328

References

Barberi, F., Dallan, L., Franzini, M., Giglia, G., Innocenti, F., Marinelli, G., Raggi, R., Ricci, C. A., Squarci, P., Taffi, L., & Trevisan, L. (1967a). Carta geologica dell'Isola d'Elba alla scala 1:25.000. E.I.R.A. *Firenze*.

Barberi, F., Dallan, L., Franzini, M., Giglia, G., Innocenti, F., Marinelli, G., Raggi, R., Squarci, P., Taffi, L., & Trevisan, L. (1969). Note illustrative della Carta Geologica d'Italia alla scala 1:100.000. Foglio 126 (Isola d'Elba). *Servizio Geologico d'Italia*, 32.

Barberi, F., Innocenti, F., & Ricci, C. A. (1967b). Il complesso scistoso di Capo Calamita (Isola d'Elba). *Atti della Società Toscana di Scienze Naturali: Serie A*, *74*, 569–617.

Bartole, R. (1995). The North tyrrhenian–Northern Apennines post-collisional system: Constraints for a geodynamic model. *Terra Nova*, *7*(1), 7–30. https://doi.org/10.1111/j.1365-3121.1995.tb00664.x

Bianco, C., Brogi, A., Caggianelli, A., Giorgetti, G., Liotta, D., & Meccheri, M. (2015). HP-LT metamorphism in Elba Island: Implications for the geodynamic evolution of the inner Northern Apennines (Italy). *Journal of Geodynamics*, *91*, 13–25. https://doi.org/10.1016/j.jog.2015.08.001

Bianco, C., Godard, G., Halton, A., Brogi, A., Liotta, D., & Caggianelli, A. (2019). The lawsonite-glaucophane blueschists of Elba Island (Italy). *Lithos*, *348*, 105198. https://doi.org/10.1016/j.lithos.2019.105198

Bodechtel, J. (1964). Stratigraphie und tektonik der schuppenzone elbas. *Geologische Rundschau*, *53*(1), 25–41. https://doi.org/10.1007/BF02040737

Bonini, M., Sani, F., Stucchi, E. M., Moratti, G., Benvenuti, M., Menanno, G., & Tanini, C. (2014). Late Miocene shortening of the Northern Apennines back-arc. *Journal of Geodynamics*, *74*, 1–31. https://doi.org/10.1016/j.jog.2013.11.002

Bortolotti, V., Fazzuoli, M., Pandeli, E., Principi, G., Babbini, A., & Corti, S. (2001). Geology of central and eastern Elba island. *Italy. Ofioliti*, *26*(2A), 97–150.

Burckhardt, C. E. (1946). Il sondaggio di belagajo (grosseto) e il suo significato geologico. *Bollettino Della Società Geologica Italiana*, *65*(1), 97–107.

Carmignani, L., Decandia, F. A., Fantozzi, P. L., Lazzarotto, A., Liotta, D., & Meccheri, M. (1994). Tertiary extensional tectonics in Tuscany (northern Apennines. *Italy). Tectonophysics*, *238*(1-4), 295–315. https://doi.org/10.1016/0040-1951(94)90061-2

Caso, F., Nerone, S., Petroccia, A., & Bonasera, M. (2021). Geology of the southern gran paradiso massif and Lower piedmont zone contact area (middle Ala valley, western Alps Italy). *Journal of Maps*, *17*(2), 237–246. https://doi.org/10.1080/17445647.2021.1911869

Cassinis, G., Perotti, C., & Santi, G. (2018). Post-Variscan verrucano-like deposits in Italy, and the onset of the alpine tectono-sedimentary cycle. *Earth-Science Reviews*, *185*, 476–497. https://doi.org/10.1016/j.earscirev.2018.06.021

Clemenzi, L., Molli, G., Storti, F., Muchez, P., Swennen, R., & Torelli, L. (2014). Extensional deformation structures within a convergent orogen: The Val di Lima low-angle normal fault system (Northern Apennines, Italy). *Journal of Structural Geology*, *66*, 205–222. https://doi.org/10.1016/j.jsg.2014.05.019

Collettini, C., & Holdsworth, R. E. (2004). Fault zone weakening and character of slip along low-angle normal faults: Insights from the Zuccale fault, elba, Italy. *Journal of the Geological Society*, *161*(6), 1039–1051. https://doi.org/10.1144/0016-764903-179

Conti, P., Cornamusini, G., & Carmignani, L. (2020). An outline of the geology of the Northern Apennines (Italy), with geological map at 1: 250,000 scale. *Italian Journal of Geosciences*, *139*(2), 149–194. https://doi.org/10.3301/IJG.2019.25

Davis, D., Suppe, J., & Dahlen, F. A. (1983). Mechanics of fold-and-thrust belts and accretionary wedges. *Journal of Geophysical Research: Solid Earth*, *88*(B2), 1153–1172. https://doi.org/10.1029/JB088iB02p01153

Decandia, F. A., Lazzarotto, A., & Liotta, D. (1993). La serie ridotta nel quadro della evoluzione geologica della Toscana meridionale. *Memorie Della Società Geologica Italiana*, *49*, 181–191.

Deschamps, Y., Dagallier, G., Macaudier, J., Marignac, C., Maine, B., & Saupé, F. (1983). Le gisement de pyrite-hématite de Valle giove (Rio Marina, Ile d'Elbe, italie). contribution à la connaissance des gisements de toscane-I. Partie 1. *Schweiz. Min. Petr. Mitt*, *63*, 149–165.

De Stefani, C. (1914). Fossili paleozoici dell'Isola d'Elba. *Rendiconti Dell'Accademia dei Lincei*, *23*, 906–913.

Dini, A., Innocenti, F., Rocchi, S., Tonarini, S., & Westerman, D. S. (2002). The magmatic evolution of the late Miocene laccolith–pluton–dyke granitic complex of Elba Island, Italy. *Geological Magazine*, *139*(3), 257–279. https://doi.org/10.1017/S0016756802006556

Di Rosa, M., De Giorgi, A., Marroni, M., & Pandolfi, L. (2017). Geology of the area between golo and tavignano valleys (central corsica): a snapshot of the continental metamorphic units of alpine corsica. *Journal of Maps*, *13*(2), 644–653. https://doi.org/10.1080/17445647.2017.1351900

Dominguez, S., Malavieille, J., & Lallemand, S. E. (2000). Deformation of accretionary wedges in response to seamount subduction: Insights from sandbox experiments. *Tectonics*, *19*(1), 182–196. https://doi.org/10.1029/1999TC900055

Dünkel, I. (2002). *The genesis of east Elba iron ore deposits and their interrelation with messinian tectonics (doctoral*

dissertation (Inst. und Museum für Geologie und Paläontologie. Universität Tübingen). http://citeseerx.ist.psu.edu/viewdoc/download?doi=10.1.1.634.787&rep=rep1&type=pdf

Duranti, S., Palmeri, R., Pertusati, P. C., & Ricci, C. A. (1992). Geological evolution and metamorphic petrology of the basal sequences of eastern Elba (complex II). *Acta Vulcanologica*, *2*, 213–229.

Ellis, S., Schreurs, G., & Panien, M. (2004). Comparisons between analogue and numerical models of thrust wedge development. *Journal of Structural Geology*, *26* (9), 1659–1675. https://doi.org/10.1016/j.jsg.2004.02.012

Franceschelli, M., Leoni, L., Memmi, I., & Puxeddu, M. (1986). Regional distribution of Al-silicates and metamorphic zonation in the low-grade Verrucano metasediments from the northern Apennines, Italy. *Journal of Metamorphic Geology*, *4*(3), 309–321. https://doi.org/10.1111/j.1525-1314.1986.tb00353.x

Frassi, C., Göncüoğlu, C. M., Marroni, M., Pandolfi, L., Ruffini, L., Ellero, A., … Sayit, K. (2016). The intra-pontide suture zone in the tosya-kastamonu area, Northern Turkey. *Journal of Maps*, *12*(sup1), 211–219. https://doi.org/10.1080/17445647.2016.1192330

Frassi, C., Musumeci, G., Zucali, M., Mazzarini, F., Rebay, G., & Langone, A. (2017). The cotoncello shear zone (Elba Island, Italy): The deep root of a fossil oceanic detachment fault in the Ligurian ophiolites. *Lithos*, *278-281*, 445–463. https://doi.org/10.1016/j.lithos.2017.02.015

Grohmann, C. H., & Campanha, G. A. C. (2010, December 13–17). *Openstereo: Open source, cross-platform software for structural geology analysis*. Presented at the AGU 2010 fall meeting, San Francisco, CA.

Gundlach-Graham, A., Garofalo, P. S., Schwarz, G., Redi, D., & Günther, D. (2018). High-resolution, quantitative element imaging of an Upper crust, Low-angle cataclasite (Zuccale fault. *Northern Apennines) by Laser Ablation ICP Time-of-Flight Mass Spectrometry. Geostandards and Geoanalytical Research*, *42*(4), 559–574. https://doi.org/10.1111/ggr.12233

Jacobs, J., Paoli, G., Rocchi, S., Ksienzyk, A. K., Sirevaag, H., & Elburg, M. A. (2018). Alps to Apennines zircon roller coaster along the Adria microplate margin. *Scientific Reports*, *8*(1), 1–8. https://www.nature.com/articles/s41598-018-20979-w

Keller, J. V. A., & Coward, M. P. (1996). The structure and evolution of the Northern Tyrrhenian Sea. *Geological Magazine*, *133*(1), 1–16. https://doi.org/10.1017/S0016756800007214

Keller, J. V. A., & Pialli, G. (1990). Tectonics of the island of elba: A reappraisal. *Bollettino Della Società Geologica Italiana*, *109*(2), 413–425.

Lippolt, H. J., Wernicke, R. S., & Bahr, R. (1995). Paragenetic specularite and adularia (elba, Italy): concordant (U + Th)–He and K-Ar ages. *Earth and Planetary Science Letters*, *132*(1-4), 43–51. https://doi.org/10.1016/0012-821X(95)00046-F

Maineri, C., Benvenuti, M., Costagliola, P., Dini, A., Lattanzi, P., Ruggieri, G., & Villa, I. M. (2003). Sericitic alteration at the La crocetta deposit (Elba Island, Italy): interplay between magmatism, tectonics and hydrothermal activity. *Mineralium Deposita*, *38*(1), 67–86. https://doi.org/10.1007/s00126-002-0279-2

Marinelli, G. (1959). Le intrusioni terziarie dell'Isola d'Elba. *Atti Della Società Toscana di Scienze Naturali, Memorie, Serie A*, *66*, 50–223.

Massa, G., Musumeci, G., Mazzarini, F., & Pieruccioni, D. (2017). Coexistence of contractional and extensional tectonics during the northern Apennines orogeny: The late Miocene out-of-sequence thrust in the Elba Island nappe stack. *Geological Journal*, *52*(3), 353–368. https://doi.org/10.1002/gj.2761

Mauffret, A., Contrucci, I., & Brunet, C. (1999). Structural evolution of the Northern Tyrrhenian Sea from new seismic data. *Marine and Petroleum Geology*, *16*(5), 381–407. https://doi.org/10.1016/S0264-8172(99)00004-5

Mazzarini, F., & Musumeci, G. (2008). Hydrofracturing-related sill and dyke emplacement at shallow crustal levels: The eastern Elba dyke complex, Italy. *Geological Society, London, Special Publications*, *302*(1), 121–129. https://doi.org/10.1144/SP302.9

Mazzarini, F., Musumeci, G., & Cruden, A. R. (2011). Vein development during folding in the upper brittle crust: The case of tourmaline-rich veins of eastern Elba Island, northern Tyrrhenian Sea, Italy. *Journal of Structural Geology*, *33*(10), 1509–1522. https://doi.org/10.1016/j.jsg.2011.07.001

Mazzarini, F., Musumeci, G., Viola, G., Garofalo, P. S., & Mattila, J. (2019). Structural and lithological control on fluid circulation, dilation and ore mineralization (Rio albano mine, Island of Elba, Italy). *Journal of Structural Geology*, *126*, 210–230. https://doi.org/10.1016/j.jsg.2019.06.012

Musumeci, G., Mazzarini, F., & Cruden, A. R. (2015). The Zuccale fault, Elba Island, Italy: A new perspective from fault architecture. *Tectonics*, *34*(6), 1195–1218. https://doi.org/10.1002/2014TC003809

Musumeci, G., Mazzarini, F., Tiepolo, M., & Di Vincenzo, G. (2011). U-Pb and 40Ar-39Ar geochronology of palaeozoic units in the northern Apennines: Determining protolith age and alpine evolution using the Calamita Schist and Ortano porphyroid. *Geological Journal*, *46* (4), 288–310. https://doi.org/10.1002/gj.1266

Musumeci, G., & Vaselli, L. (2012). Neogene deformation and granite emplacement in the metamorphic units of northern Apennines (Italy): insights from mylonitic marbles in the Porto Azzurro pluton contact aureole (Elba island). *Geosphere*, *8*(2), 470–490. https://doi.org/10.1130/GES00665.1

Orndorff, R. C., Stamm, N., Craigg, S., Edwards, L., Fullerton, D., Murchey, B., … Tew, B. N. (2007). Divisions of geologic time–major chronostratigraphic and geochronologic units. *US Geol Surv Fact Sheet*, *3015*(2). http://web.csulb.edu/~rodrigue/geog442/USGStimescaleFS10-3059.pdf

Papeschi, S., Iaccarino, S., & Montomoli, C. (2020a). Underthrusting and exhumation of continent-derived units within orogenic wedge: An example from the Northern Apennines (Italy). *Journal of Maps*, *16*(2), 638–650. https://doi.org/10.1080/17445647.2020.1795736

Papeschi, S., Musumeci, G., Massonne, H. J., Bartoli, O., & Cesare, B. (2019). Partial melting and strain localization in metapelites at very low-pressure conditions: The northern Apennines magmatic arc on the Island of Elba, Italy. *Lithos*, *350*, 105230. https://doi.org/10.1016/j.lithos.2019.105230

Papeschi, S., Musumeci, G., Massonne, H. J., Mazzarini, F., Ryan, E., & Viola, G. (2020b). High–pressure ($P = 1.5$–1.8 GPa) blueschist from elba: Implications for underthrusting and exhumation of continental units in the Northern Apennines. *Journal of Metamorphic Geology*, *38*(5), 495–525. https://doi.org/10.1111/jmg.12530

Papeschi, S., Musumeci, G., & Mazzarini, F. (2017). Heterogeneous brittle-ductile deformation at shallow crustal levels under high thermal conditions: The case of a synkinematic contact aureole in the inner northern

Apennines, southeastern Elba Island, Italy. *Tectonophysics*, *717*, 547–564. https://doi.org/10.1016/j.tecto.2017.08.020

Papeschi, S., Musumeci, G., & Mazzarini, F. (2018). Evolution of shear zones through the brittle-ductile transition: The Calamita Schists (Elba Island, Italy). *Journal of Structural Geology*, *113*, 100–114. https://doi.org/10.1016/j.jsg.2018.05.023

Perrin, M. (1975). L'Ile d'Elbe et la limite alpes-apennin: Données sur la structure géologique et l'évolution tectogénétique de l'Elbe alpine et de l'Elbe apennine. *Bollettino Della Società Geologica Italiana*, *94*, 1929–1955.

Perrin, M., & Neumann, M. (1970). Présence, au NE de l'Ile d'Elbe d'une série de type "scisti policromi" à faune maestrichtienne. *C.R. Acad. Sci., Sér. D*, *270*, 2260–2263.

Pertusati, P. C., Raggi, G., Ricci, C. A., Duranti, S., & Palmeri, R. (1993). Evoluzione post-collisionale dell'Elba centro-orientale. *Memorie Della Società Geologica Italiana*, *49*, 297–312.

Platt, J. P. (1986). Dynamics of orogenic wedges and the uplift of high-pressure metamorphic rocks. *Geological Society of America Bulletin*, *97*(9), 1037–1053. https://doi.org/10.1130/0016-7606(1986)97<1037:DOOWAT>2.0.CO;2

Principi, G., Bortolotti, V., Pandeli, E., Fanucci, F., Benvenuti, M., Chiari, M., Dini, A., Fazzuoli, M., Menna, F., Morelli, D., Moretti, S., Nirta, G., & Reale, V. (2015). Note Illustrative della Carta Geologica d'Italia alla scala 1:50.000. Foglio 316, 317, 328, 329 - Isola d'Elba. *Servizio Geologico d'Italia, Rom*a, 263 pp.

Ramsay, J. G., & Huber, M. I. (1987). *The techniques of modern structural geology*. Academic Press.

Reutter, K. J., & Spohn, A. (1982). The position of the west-Elba ophiolites within the tectonic framework of the Apennines. *Ofioliti*, *7*, 467–478.

Ryan, E., Papeschi, S., Viola, G., Musumeci, G., Mazzarini, F., Torgersen, E., … Ganerød, M. (2021). Syn-orogenic exhumation of high-P units by upward extrusion in an accretionary wedge: Insights from the eastern Elba nappe stack (Northern Apennines, Italy). *Tectonics*, *40*(5), e2020TC006348. https://doi.org/10.1029/2020TC006348

Siivola, J., & Schmid, R.. (2007). List of mineral abbreviations. In D. Fettes & J. Desmons (Eds.), *Metamorphic Rocks: A classification and Glossary of Terms. Recommendations of the International Union of Geological Sciences Subcommission on the Systematics of Metamorphic Rocks*. Cambridge University Press.

Siniscalchi, A., Diaferia, I., Liuni, M. P., Loddo, M., Magrì, C., Moretti, P., … Tripaldi, S. (2008, August). Integrated geophysical approach for imaging the Porto Azzurro (Elba, Italy) plutons and the associated structures. In Oslo, Proceedings 33rd International Geological Congress (pp. 6-14).

Sirevaag, H., Jacobs, J., Ksienzyk, A. K., Rocchi, S., Paoli, G., Jørgensen, H., & Košler, J. (2016). From Gondwana to Europe: The journey of Elba Island (Italy) as recorded by U–Pb detrital zircon ages of Paleozoic metasedimentary rocks. *Gondwana Research*, *38*, 273–288. https://doi.org/10.1016/j.gr.2015.12.006

Tanelli, G., Benvenuti, M., Costagliola, P., Dini, A., Lattanzi, P., Maineri, C., … Ruggieri, G. (2001). The iron mineral deposits of Elba Island: State of the art. *Ofioliti*, *26*(2a), 239–248.

Trevisan, L. (1950). L'Elba orientale e la sua tettonica di scivolamento per gravità. *Memorie Dell'Istituto Geologico Dell'Università di Padova*, *16*, 5–39.

Viola, G., Torgersen, E., Mazzarini, F., Musumeci, G., van der Lelij, R., Schönenberger, J., & Garofalo, P. S. (2018). New constraints on the evolution of the inner Northern Apennines by K-Ar dating of late miocene-early Pliocene compression on the Island of Elba, Italy. *Tectonics*, *37*(9), 3229–3243. https://doi.org/10.1029/2018TC005182

Viti, C., & Mellini, M. (1998). Mesh textures and bastites in the Elba retrograde serpentinites. *European Journal of Mineralogy*, *10*(6), 1341–1359. https://doi.org/10.1127/ejm/10/6/1341

Wallis, S. R., Platt, J. P., & Knott, S. D. (1993). Recognition of syn-convergence extension in accretionary wedges with examples from the calabrian Arc and the eastern Alps. *American Journal of Science*, *293*(5), 463–494. https://doi.org/10.2475/ajs.293.5.463

Zitzmann, A. (1977). The iron ore deposits of Europe and adjacent areas. *Bundesanstalt Fuer Geowissenschften und Rohstoffe, Hannover*.